

CONFIDENTIAL

Copy 317  
RM 156806

N 63 20 5 26

NACA

# RESEARCH MEMORANDUM

TRANSONIC FLUTTER INVESTIGATION OF AN ALL-MOVABLE  
HORIZONTAL TAIL FOR A FIGHTER AIRPLANE

By Norman S. Land and Frank T. Abbott, Jr.

Langley Aeronautical Laboratory  
Langley Field, Va.

OTS PRICE

ROX \$ 2.60

CROFILM \$ 0.95

CLASSIFICATION CHANGED FROM  
CONFIDENTIAL TO UNCLASSIFIED--  
AUTHORITY NASA-CCN 5-EFFECTIVE  
17 JULY 83, JIM CARROLL  
DOC. INC.

NATIONAL ADVISORY COMMITTEE  
FOR AERONAUTICS

WASHINGTON

January 14, 1957

DECLASSIFIED

## NATIONAL ADVISORY COMMITTEE FOR AERONAUTICS

## RESEARCH MEMORANDUM

TRANSONIC FLUTTER INVESTIGATION OF AN ALL-MOVABLE  
HORIZONTAL TAIL FOR A FIGHTER AIRPLANE

By Norman S. Land and Frank T. Abbott, Jr.

## SUMMARY

20526

A transonic flutter investigation was made of a model of an all-movable horizontal tail for a fighter airplane. The model had an aspect ratio of 3.3, a taper ratio of 0.42, and  $35^\circ$  of sweepback of the quarter-chord line. Analytical and experimental studies were made of the effect on the flutter speed of various ratios of panel bending frequency to pitching frequency. It was found that the flutter speed is lowered considerably below the fixed-root value when the ratio of bending frequency to pitching frequency is near 1.0. In the range of low flutter speeds, an increase in structural damping had a beneficial effect. The effect of the Mach number on the flutter speed varied with the ratio of bending frequency to pitching frequency for the values tested between 1.05 and 0.50. The greatest effect was shown for the lowest frequency ratio.

## INTRODUCTION

The transonic flutter boundaries of simple, geometrically similar models of the wing and horizontal tail of a new fighter airplane have been under study in the Langley transonic blowdown tunnel. Results of the investigation of the wing are reported in reference 1. The present report presents the results of the zero-lift flutter characteristics of a model of the all-movable horizontal tail of the airplane. Since very little flutter information has been published to date on all-movable tails, the present experimental investigation was made as broad as possible with the model available. An analytical investigation was also made, and the results are compared with those of the experimental investigation.

The tail model had an aspect ratio of 3.3, a taper ratio of 0.42,  $35^\circ$  of sweepback of the quarter-chord line, airfoil sections tapering from 6 percent thick at the root to 4 percent thick at the tip, and a rounded tip. The pitch axis was located at 78.9 percent of the chord in the plane of symmetry. The tests covered a range of Mach numbers

from 0.6 to 1.3, a range of Reynolds numbers from approximately  $2.0 \times 10^6$  to  $6.5 \times 10^6$  (based on streamwise root chord), and a range of mass ratios from 30 to 94.

## SYMBOLS

a	distance perpendicular to elastic axis, in tail half-chord, from midchord to elastic-axis position; positive when elastic axis is rearward of midchord
b	half-chord perpendicular to elastic axis, ft
EI	bending stiffness, lb-in. <sup>2</sup>
GJ	torsional stiffness, lb-in. <sup>2</sup>
g	damping coefficient
$I_\alpha$	mass moment of inertia per unit length of tail section about elastic axis, slug-ft <sup>2</sup> /ft
M	Mach number
m	mass of tail per unit length along elastic axis, slugs/ft
q	dynamic pressure, lb/sq in.
$r_\alpha$	nondimensional radius of gyration of tail section about elastic axis, $\left(\frac{I_\alpha}{mb^2}\right)^{1/2}$
V	stream velocity, ft/sec
$V_n$	velocity normal to elastic axis, ft/sec
$x_\alpha$	distance perpendicular to elastic axis in tail half-chord from elastic axis to center of gravity; positive when center of gravity is rearward of elastic axis
$\eta$	nondimensional coordinate along elastic axis, fraction of length
$\mu$	mass-ratio parameter, $\frac{m}{\pi \rho b^2}$

$\rho$  mass density of air, slugs/cu ft  
 $\omega$  angular frequency of vibration, radians/sec

Subscripts:

e experimental values  
h bending  
R calculated values  
r reference-chord values ( $\eta = 0.75$ )  
 $\alpha$  torsion  
 $\phi$  pitching


## MODEL AND APPARATUS

### Model

The horizontal-tail model had an aspect ratio of 3.3, a taper ratio of 0.42,  $35^\circ$  of sweepback of the quarter-chord line, NACA 65A-series airfoil sections tapering from 6 percent thick at the root to 4 percent thick at the tip, and rounded tips. The pitch axis was located at 78.9 percent of the chord in the plane of symmetry. The linear dimensions of the model were scaled down from the dimensions of the horizontal tail of the airplane. No attempt was made to construct a complete dynamic model of the airplane tail. Dimensions of the model are shown in figure 1.

Actually, two models were constructed and tested but, since they were substantially identical, they are referred to as one. The model was moulded from fiber glass and plastic. Two layers of woven fiber glass, each 0.004 inch thick, formed the outer skin of the model, and the interior was filled with fiber glass roving running lengthwise of the panel. The whole model was impregnated with plastic. The panel strain gages, sensitive to bending and torsion, were moulded in the panels just under the skin near the root of each panel.

The model was mounted in a cylindrical fuselage in the Langley transonic blowdown tunnel which has a 26-inch octagonal test section (refs. 1 to 3). Figure 2 is a sketch of a model in the tunnel. Although not shown in figure 2, the downstream end of the fuselage was rigidly attached to a support strut. The natural frequency of the fuselage, as assembled in the tunnel, was 12.4 cycles per second. For the present



investigation the tail model was mounted on the fuselage in such a manner as to allow a limited amount of freedom in pitch relative to the fuselage. The important features of this mounting are illustrated in figure 3 which gives a schematic cross-sectional view in the plane of symmetry of the mounting fixture. Figure 4 shows the model in the partially assembled fixture, and figure 5 shows it in the fully assembled fixture. This method of mounting the model allowed it to pitch about an axis fixed by the journal bearing (at 78.9 percent of the chord in the plane of symmetry). The extent of the pitch motion was limited by adjustable stops. The stiffness and the natural frequency in the pitch degree of freedom were adjustable by control of the active length of a cantilever spring. A strain gage mounted on the pitch spring gave a signal proportional to the pitch deflection. No freedom was allowed in roll, yaw, or translation.

#### Measurement of Physical Properties of Model

The lowest natural frequencies of the panels of the model and the associated node lines are shown in figure 6. These were determined with the model mounted in the test fixture but having no pitch freedom. The methods used in obtaining these data are described in references 1 and 2.

The other physical properties of the panels of the tail are given in table I. Bending and torsional stiffnesses  $EI$  and  $GJ$  were determined from the load-deflection curves of a tail panel in bending and torsion. The mass, center-of-gravity location, and radius of gyration were determined for each of ten segments which were sawed out perpendicular to the elastic axis of the model after completion of the tests. Details of the methods of measuring these parameters are given in references 1 and 2.

It was considered desirable to describe the pitch degree of freedom in terms of the uncoupled pitch frequency. The uncoupled characteristics of the complete model in pitch could not be determined, however, because of the large amount of coupling between pitching and panel bending and torsion. Therefore, a dummy model was constructed which consisted only of a center section of the tail with no panels attached. This dummy was ballasted with weights to have the same moment of inertia about the pitch axis as the complete flutter model. The moment of inertia of the complete model about the pitch axis was determined to be  $0.000296 \text{ slug-ft}^2$  by swinging it as a compound, or physical, pendulum. The moment of inertia of the dummy model was adjusted to the value of the complete model.

Because of the rapid decay of free pitching oscillations a response-curve method was employed to determine the frequency and damping. This method is based on the fact that, for forced oscillations of a

single-degree-of-freedom system with small damping, the frequency at peak response can be taken as the undamped natural frequency, and the "sharpness" of the response curve is a measure of the damping of the system. Reference 4 gives the relations between response-curve width and the damping coefficient used in the flutter calculations. Pitching vibrations were excited by an electrodynamic vibrator driven by an audio oscillator. Vibration amplitude was measured with an optical system of fairly large magnification. It was soon discovered that the damping coefficient decreased somewhat as the amplitude of vibration increased. Consequently, all determinations were made by holding a constant low-vibration amplitude (approximately  $0.07^\circ$ , peak to peak) and measuring the vibrator current as the driving frequency was varied through the resonant frequency. Since the panel bending and torsion frequencies were widely separated, the damping of one of the tail panels (no pitch freedom) in bending and torsion was also measured by the response-curve technique. A typical set of nondimensional response curves for pitch, bending, and torsion together with the derived values of  $g_\phi$ ,  $g_h$ , and  $g_\alpha$  are given in figure 7. It is believed that this method is fairly reliable because the damping in the panel bending mode so obtained agrees well with a value determined from records of the decay of free bending oscillations.

### Instrumentation

Airstream information (stagnation pressure, stagnation temperature, and test-section static pressure) and the outputs of strain gages indicating bending, torsional, and pitching motions of the model were recorded on a multichannel oscillograph as a time history of each run. A subsequent examination was made of each record to determine the point representing the onset of sustained flutter. Since there was not much intermittent flutter, the flutter point was easily determined by visual inspection of each record. The instrumentation used was essentially the same as has been described in references 1 and 2, except that the additional channel of pitch information was added.

### EXPERIMENTAL TEST PROCEDURE

A few preliminary tests showed that the amplitude of flutter would have to be limited to a low value to prevent frequent pitch-spring breakage. The majority of the tests were made with the stop screws set so that the model could pitch approximately  $\pm \frac{1}{2}^\circ$ . Before each test run, it was made certain that the model was clear of the pitch stops, and efforts were made to insure that the model was trimmed for zero aerodynamic moment; however, it is not entirely certain that the model was

off the stops at the onset of flutter. Presumably, because of the restricted amplitude in pitch, the amplitude of the motion at the onset of flutter was relatively small, and no model destruction was encountered.

In order to detect the onset of flutter during the tests, the amplified signals from one panel-bending strain gage and the pitch-spring strain gage were applied to an oscilloscope. The panel-bending signal was applied to the vertical-deflection system of the oscilloscope, and the pitching signal was applied to the horizontal-deflection system. This method of presentation gave a clearly recognizable indication of flutter. Buffeting, or forced oscillations resulting from tunnel turbulence, caused a random, jumbled pattern on the oscilloscope. Steady flutter resulted in a simple Lissajous figure since pitching and bending occur at the same frequency during flutter.

#### ANALYTICAL PROCEDURE

Flutter calculations were made for the model and were compared with the experimental results. In addition, the calculations were extended well beyond the range of the experimental results in order to explore regions not feasible to simulate with the present model.

The calculations were made with the aid of automatic, punched-card computing equipment and, in general, followed procedures previously reported in reference 5. The flutter mode was represented by three uncoupled degrees of freedom in the calculations: first mode bending, first mode torsion, and rigid-body pitching. Incompressible, two-dimensional aerodynamic forces and moments were taken normal to the elastic axis of the panel. The  $F$  and  $G$  functions were assumed to be constant along the span and to have values determined by the reduced frequency  $\frac{b\omega}{V}$  at the  $\eta = 0.75$  station. All other functions involving the reduced frequency were weighted according to wing taper. The uncoupled panel modes of vibration were represented by the uncoupled first bending and torsion modes of a uniform cantilever beam. The uncoupled panel frequencies were taken as the measured values given in figure 6.

The calculations covered a range of the ratio of bending frequency to pitching frequency from 0 to 2.0. The ratio of panel bending frequency to torsion frequency was maintained at a constant value (0.305) for all the calculations. The majority of the calculations were made under the assumption that the structural damping in all three modes of vibration were equal. A few cases were analyzed with a value of damping in each mode which approximated the individual values measured on the model.

DECLASSIFIED

The calculations were made over a range of airstream densities  $\rho$  from 0.00200 to 0.00432 slug/cu ft where a comparison with the experimental results was to be made. All other calculations were made with only one value of airstream density ( $\rho = 0.00200$  slug/cu ft).

## RESULTS AND DISCUSSION

### Analytical Results

The significant parts of the analytical results are presented in figures 8 and 9. Figure 8 shows some typical variations of the structural damping coefficient required for flutter  $g$  as a function of the reduced normal speed  $\frac{V_n}{b\omega_\phi}$  for several values of the ratio of bending frequency to pitching frequency. The three curves in figure 8 represent the different roots of the flutter stability determinant. The reduced streamwise flutter speed  $\frac{V}{b\omega_\alpha}$  is shown in figure 9 as a function of the frequency ratio  $\frac{\omega_h}{\omega_\phi}$  for several values of the structural damping coefficient. A comparison of figures 8 and 9 indicates that the lower flutter boundary up to  $\frac{\omega_h}{\omega_\phi} \approx 1.0$  is determined by the curve with square-shaped symbols in figure 8. The loop in the flutter boundary between values of  $\frac{\omega_h}{\omega_\phi}$  of 0.6 and 1.0 is seen to result from a second crossing of the  $g = 0$  axis by the curve with square-shaped symbols in figure 8. The existence of a second neutrally stable mode is indicated in figure 8(c) by the crossing of the  $g = 0$  axis by the curve with diamond-shaped symbols. As indicated by figures 8(d) and 8(e), this mode becomes the lowest and only neutrally stable mode for  $\frac{\omega_h}{\omega_\phi} > 1.0$ . The presence of a flutter boundary, determined by the curves in figure 8 with diamond-shaped symbols, was indicated by the calculations to exist for values of  $\frac{\omega_h}{\omega_\phi}$  somewhat less than 0.7. The correct form for this boundary, however, was rather obscure and has not been presented since the flutter speeds were, in all cases, higher than those given in figure 9.

The analytical results showed that the lowest flutter-speed coefficient was obtained at a value of the ratio of uncoupled bending frequency to pitching frequency of 0.85 if the structural damping were zero, and at



a ratio of 0.7 if the damping coefficient were 0.3. At the critical frequency ratios, the flutter speed was reduced to 32 percent of the fixed-root value for zero structural damping, and to 66 percent of the fixed-root value if the structural damping coefficient were 0.3. As the frequency ratio is increased, the flutter-speed coefficient jumps to a higher value corresponding to a different flutter mode. Further increases in frequency ratio are seen to have little effect on the flutter-speed coefficient. The value of the structural damping coefficient is seen in figure 9 to have a large effect on the flutter-speed coefficient in the range of frequency ratios  $\frac{\omega_h}{\omega_\phi}$  between 0.6 and 1.0. The value of 0.3 corresponds to that obtained in the pitching degree of freedom (fig. 7) for the experimental model. When measured values of damping are used, as indicated by the circular symbols in figure 9, the results are approximately the same as those for  $g = 0.1$  for all degrees of freedom.

Because of the results presented in figure 9, a question is raised as to the structural parameters of the tail which have the greatest effect on the flutter speed. For values of  $\frac{\omega_h}{\omega_\phi}$  greater than 1.0, the flutter speed is directly proportional to the uncoupled panel torsion frequency  $\omega_\alpha$ . For values of the frequency ratio below 1.0, the situation is somewhat more complicated. The calculations were made for a fixed value of the ratio of panel bending frequency to torsion frequency  $\frac{\omega_h}{\omega_\alpha}$ . Thus, an increase in torsion frequency alone causes a point on the flutter boundary to be displaced to the right. The effect of the torsion frequency on the flutter speed depends, therefore, on the value of  $\frac{\omega_h}{\omega_\phi}$ . Increases in only the pitching frequency are seen to raise the flutter speed between values of the frequency ratio  $\frac{\omega_h}{\omega_\phi}$  of approximately 0.8 to 0.3.

#### Experimental Results and Comparison With Theory

The experimental flutter results are given in table II and are plotted in figure 10 which shows the flutter-speed ratio  $\frac{V_e}{V_R}$  as a function of Mach number for various experimental values of the frequency ratio  $\frac{\omega_h}{\omega_\phi}$ . The reference flutter speeds used were selected from the calculated flutter speeds at an air density and a frequency ratio corresponding to the experimental values and for an arbitrarily chosen structural damping value of  $g = 0.3$  in all three modes.

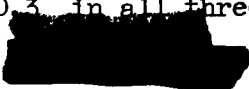


Figure 10 indicates that the variation in the flutter-speed ratio with Mach number depends on the frequency ratio, with the Mach number having the greatest effect at the lowest frequency ratio tested. At low Mach numbers the experimental and theoretical results agree fairly well ( $\frac{V_e}{V_R}$  values near 1.0) for the three lowest frequency ratios  $\frac{\omega_n}{\omega_\phi}$  of 0.50, 0.625, and 0.775. With the higher frequency ratios of 0.94 and 1.05, however, the experimental flutter speeds are less than one-half of the speeds predicted by the calculations. This is due to the fact that the model did not experience the change in flutter mode indicated by the theoretical analysis shown in figure 9. Values of the ratio of bending frequency to pitching frequency approaching 1.0 are, therefore, undesirable for the present configuration for two reasons: flutter speeds are low, and the increase in flutter speed with increasing Mach number, as usually obtained in the transonic range with fixed-root conditions, is reduced.

A somewhat more illustrative comparison between theory and experiment is shown in figure 11. The theoretical curves in figure 11 are portions of those shown in figure 9. The experimental curve shown in figure 11 represents the faired test data at a Mach number of 0.8 corrected to an air density of 0.0020 slug/cu ft (the air density of the calculations). This density correction was made on the basis of the assumption that the experimental flutter-speed coefficients varied with the mass ratio  $\mu$  in the manner shown by the analytical results. It may be seen that up to a frequency ratio of 0.75 the experimental curve agrees very well with the theoretical curve calculated for a structural damping value of 0.3 in all three modes. Above a frequency ratio of 0.75, the experimental curve departs rapidly from the theoretical curve. At the highest frequency ratio tested, the high flutter speed predicted by theory was not attained. In this connection, it should be pointed out that some unpublished flutter calculations made for the model by the aircraft manufacturer, whose airplane this model represents, showed the same general trend as the calculated results given herein. However, the manufacturer's calculations were made by a coupled mode analysis and showed the sudden increase in flutter speed to occur at a bending-pitch frequency ratio greater than 1.1. Thus, in this case at least, the use of a coupled mode analysis appears to give more realistic results than does the uncoupled analysis in the range of frequency ratios near 1.0.

### CONCLUSIONS

An analytical and experimental flutter investigation of a model of an all-movable horizontal tail for a fighter airplane led to the following conclusions:

03:12:10

1. The analytical results, which were based on the use of uncoupled models, showed that the lowest flutter-speed coefficient was obtained at a value of the ratio of uncoupled bending frequency to pitching frequency of 0.85 if the structural damping were zero, and at a ratio of 0.7 if the damping coefficient were 0.3. At the critical frequency ratios, the flutter speed was reduced to 32 percent of the fixed-root value for zero structural damping and to 66 percent of the fixed-root value if the structural damping coefficient were 0.3.

2. The experimental flutter speeds agreed well with the calculated flutter speeds at a Mach number of 0.8 and at ratios of bending frequency to pitching frequency between 0.50 and 0.75 when using a structural damping coefficient of 0.3. At higher frequency ratios the model did not experience a change in flutter mode and a high flutter speed as predicted by theory.

3. The experimental data indicated that the largest increase in flutter speed with Mach number in the transonic range occurred at the lowest value of the ratio of bending frequency to pitching frequency, 0.5, that was tested.

Langley Aeronautical Laboratory,  
National Advisory Committee for Aeronautics,  
Langley Field, Va., June 20, 1956.

DECLASSIFIED

## REFERENCES

1. Land, Norman S., and Abbott, Frank T., Jr.: Transonic Flutter Investigation of a Fighter-Airplane Wing Model and Comparison With a Systematic Plan-Form Series. NACA RM L55B16, 1955.
2. Unangst, John R., and Jones, George W., Jr.: Some Effects of Sweep and Aspect Ratio on the Transonic Flutter Characteristics of a Series of Thin Cantilever Wings Having a Taper Ratio of 0.6. NACA RM L55I13a, 1955.
3. Bursnall, William J.: Initial Flutter Tests in the Langley Transonic Blowdown Tunnel and Comparison With Free-Flight Flutter Results. NACA RM L52K14, 1953.
4. Scanlan, Robert H., and Rosenbaum, Robert: Introduction to the Study of Aircraft Vibration and Flutter. The Macmillan Co., 1951, pp. 76 and 77.
5. Barmby, J. G., Cunningham, H. J., and Garrick, I. E.: Study of Effects of Sweep on the Flutter of Cantilever Wings. NACA Rep. 1014, 1951. (Supersedes NACA TN 2121.)

TABLE I.- PHYSICAL PROPERTIES OF TAIL PANELS

$\eta$	$\frac{b}{b_r}$	$\frac{a}{a_r}$	$\frac{x_a}{x_{a_r}}$	$\frac{r_a^2}{r_{a_r}^2}$	$\frac{m}{m_r}$	EI	GJ
0.05	1.6196	-6.7193	0.0056	0.903	3.033	-----	-----
.15	1.5312	-6.0000	.1009	.933	2.651	-----	-----
.25	1.4420	-5.1842	.2085	.957	2.313	7,170	5,650
.35	1.3528	-4.2105	.3363	.972	2.003	5,670	4,220
.45	1.2652	-3.2018	.4675	.980	1.710	4,300	3,000
.55	1.1768	-2.0526	.6177	.983	1.453	3,000	2,000
.65	1.0884	-.6930	.7848	.990	1.222	1,930	1,270
.75	1.0000	1.0000	1.0000	1.000	1.000	1,200	730
.85	.9116	2.9649	1.2567	1.054	.810	750	410
.95	.8232	5.2719	1.5583	1.124	.650	520	220

$$b_r = 0.1233 \text{ foot}$$

$$x_{a_r} = -0.0892$$

$$m_r = 0.00762 \text{ slug/ft}$$

$$a_r = 0.0114$$

$$r_{a_r}^2 = 0.2530$$

TABLE II.- EXPERIMENTAL AND ANALYTICAL RESULTS

$\frac{\omega_h}{\omega_0}$	$\rho_e$ , slugs/cu ft	$q_e$ , lb/sq in.	$M_e$	$V_e$ , ft/sec	$\omega_e$ , radians/sec	$\frac{V_e}{b_r \omega_e}$	$\frac{V_e}{b_r \omega_0}$	$\frac{V_e}{V_R}$	$\mu_e$
0.50	0.00370	18.76	1.248	1,207	1,067	4.05	6.35	1.40	43.2
	.00372	19.44	1.298	1,226	1,080	4.11	6.46	1.44	43.0
	.00373	12.96	.977	1,000	960	3.36	5.26	1.17	42.8
	.00377	16.51	1.132	1,121	1,099	3.76	5.90	1.315	42.4
	.00387	18.57	1.214	1,175	1,049	3.94	6.19	1.39	41.3
	.00432	10.99	.826	836	948	2.81	4.40	1.02	37.0
.625	.00254	9.21	.999	1,022	950	3.43	6.79	1.15	62.9
	.00260	9.36	1.015	1,018	941	3.42	6.77	1.15	61.5
	.00278	7.99	.882	909	897	3.05	6.04	1.05	57.4
	.00278	7.90	.877	904	898	3.03	6.01	1.05	57.4
	.00284	8.56	.919	931	898	3.12	6.19	1.09	56.2
	.00350	9.34	1.006	877	974	2.94	5.83	1.09	45.6
.775	.00170	7.07	1.115	1,092	985	3.30	8.57	1.04	93.9
	.00170	7.05	1.110	1,078	985	3.26	8.48	1.02	93.9
	.00220	7.34	.987	989	1,004	2.98	7.75	1.04	72.5
	.00240	7.16	.906	920	960	2.78	7.24	1.00	66.5
	.00290	7.41	.838	855	973	2.58	6.71	1.00	55.0
	.00360	7.37	.749	771	1,037	2.33	6.06	.98	41.0
	.00400	6.83	.675	703	992	2.12	5.51	.93	39.9
	.00540	7.30	.603	623	992	1.88	5.45	.93	29.6
.940	.00220	4.97	.760	806	840	2.70	7.96	.40	72.5
	.00222	5.15	.777	817	847	2.74	8.08	.41	71.9
	.00260	4.79	.683	727	---	2.44	7.19	.39	61.4
	.00262	5.40	.727	769	847	2.58	7.60	.41	61.0
	.00271	5.57	.736	770	854	2.58	7.66	.42	59.0
1.05	.00204	5.74	.847	900	835	3.02	11.02	.45	78.3
	.00206	6.20	.881	931	860	3.12	11.38	.47	77.5
	.00239	6.04	.796	852	835	2.86	10.42	.46	66.8
	.00263	6.42	.793	837	847	2.81	10.24	.47	60.7
	.00266	6.28	.779	824	835	2.76	10.07	.46	60.0
	.00268	4.47	.643	692	765	2.32	8.46	.39	59.6

0313129 1930

NACA RM L56G06

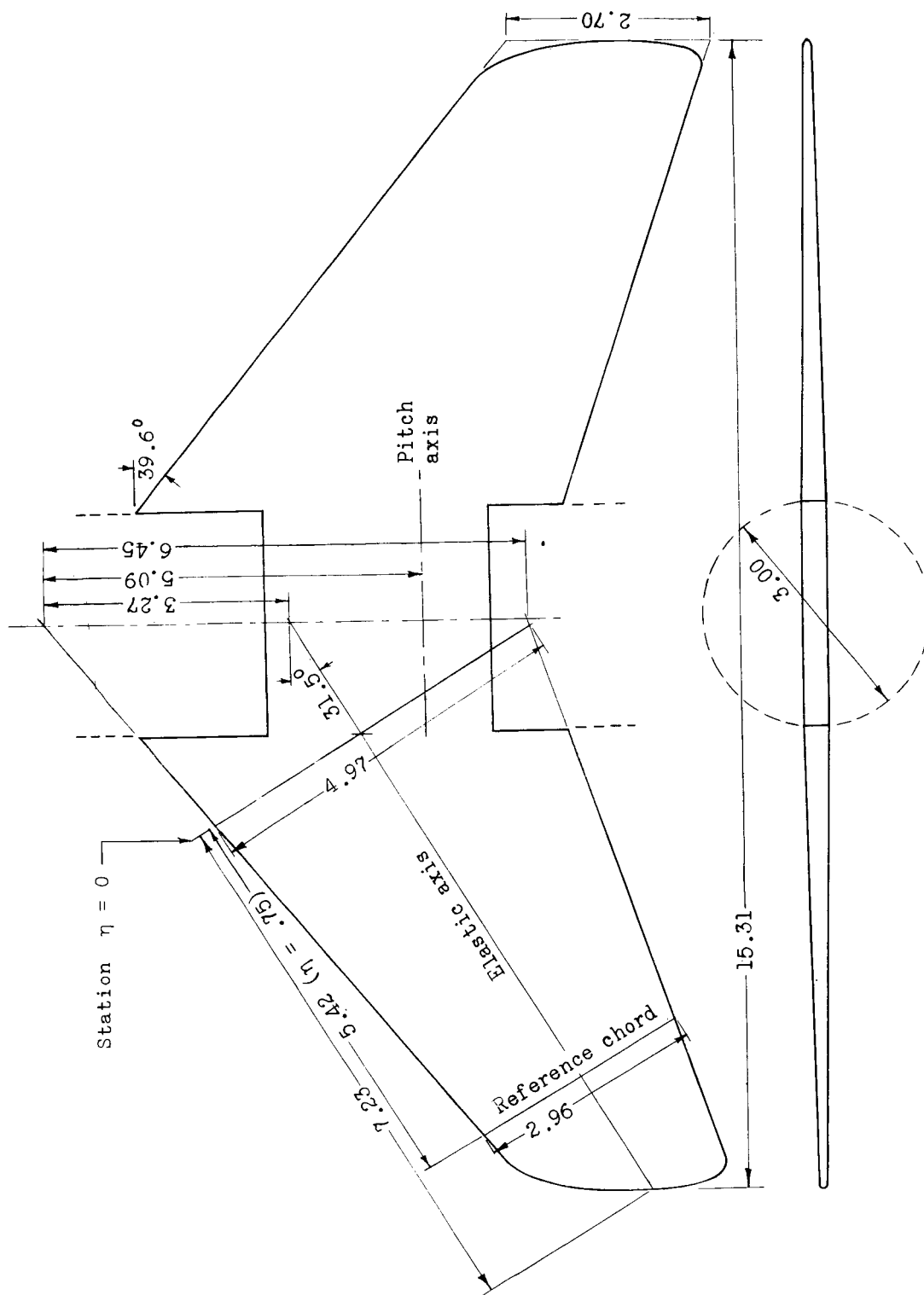


Figure 1.- Horizontal-tail flutter model. Dimensions are in inches.

REF ID: A60100

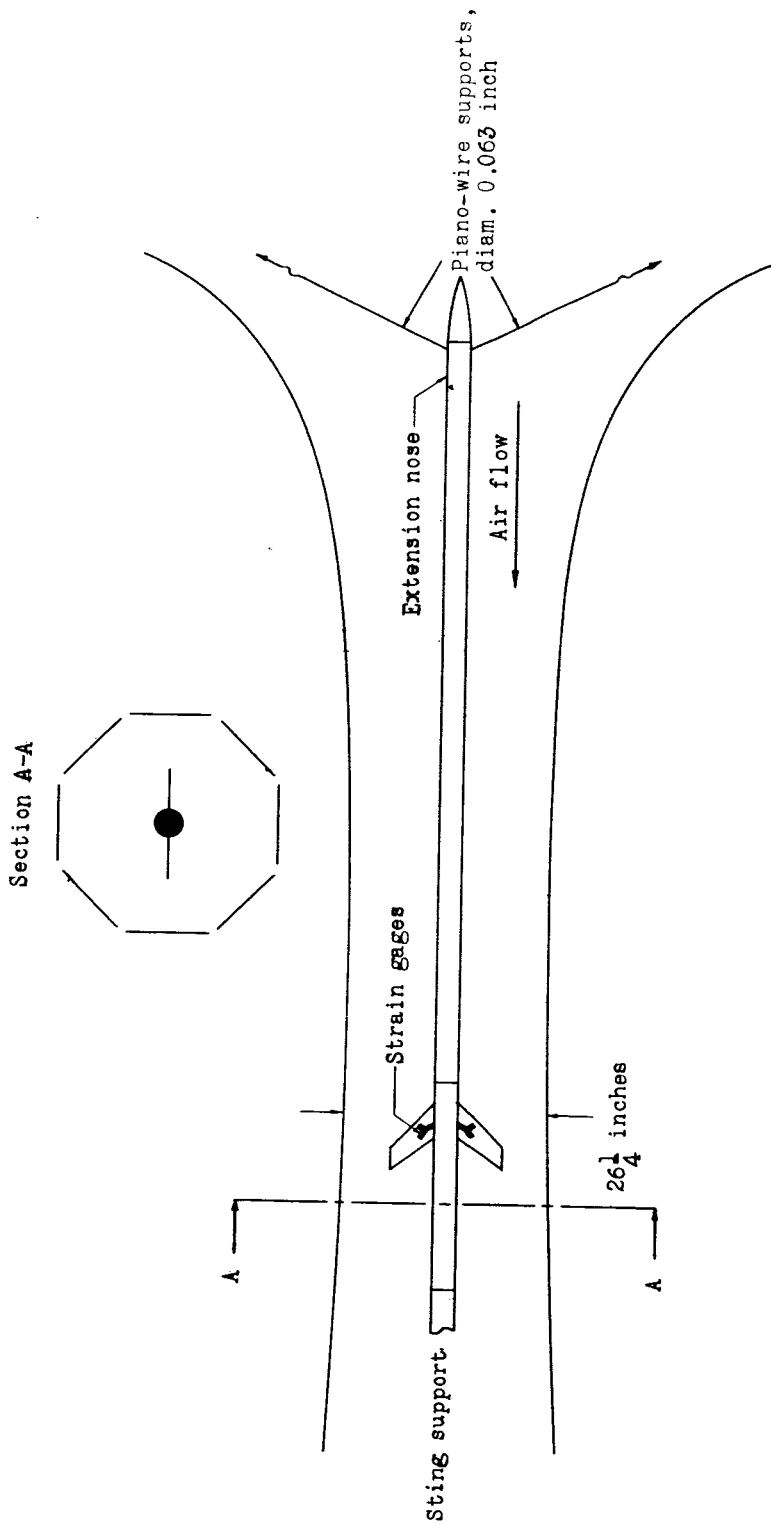


Figure 2.- Plan view of the Langley transonic blowdown tunnel with flutter model installed.



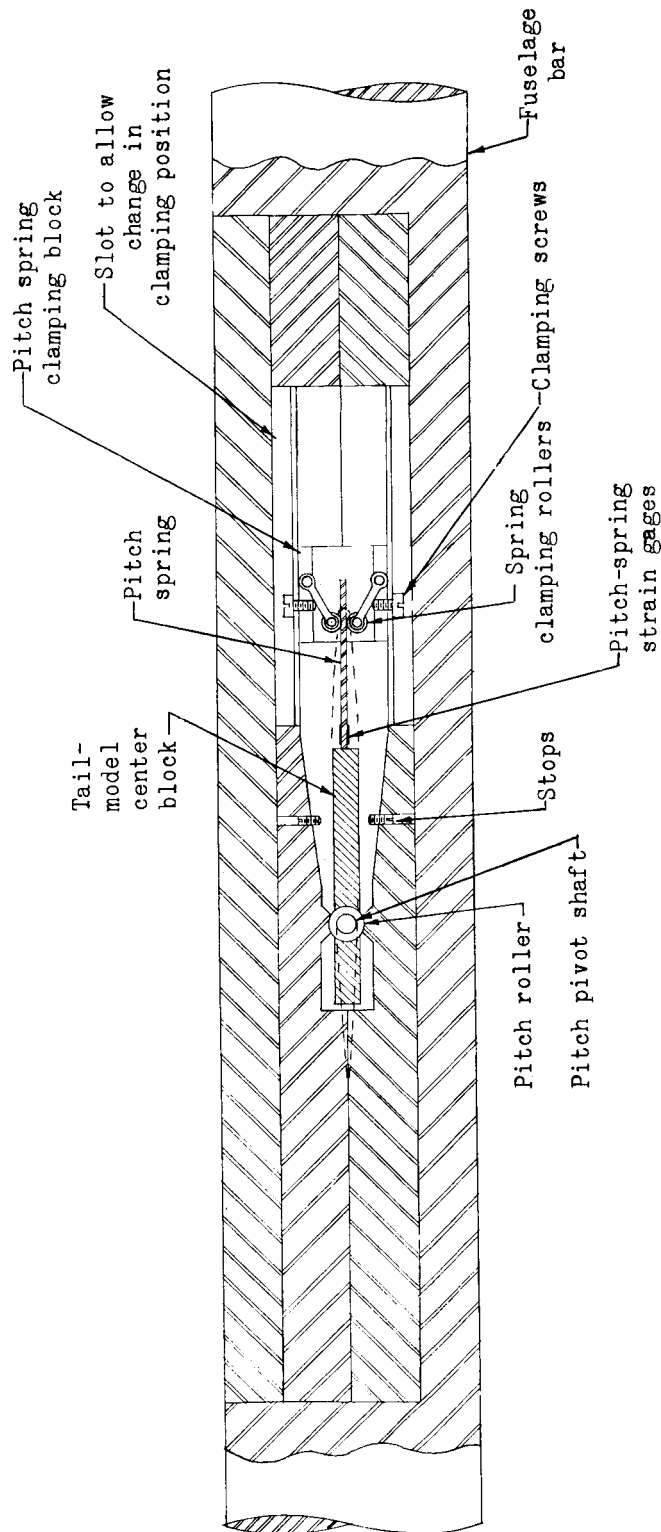
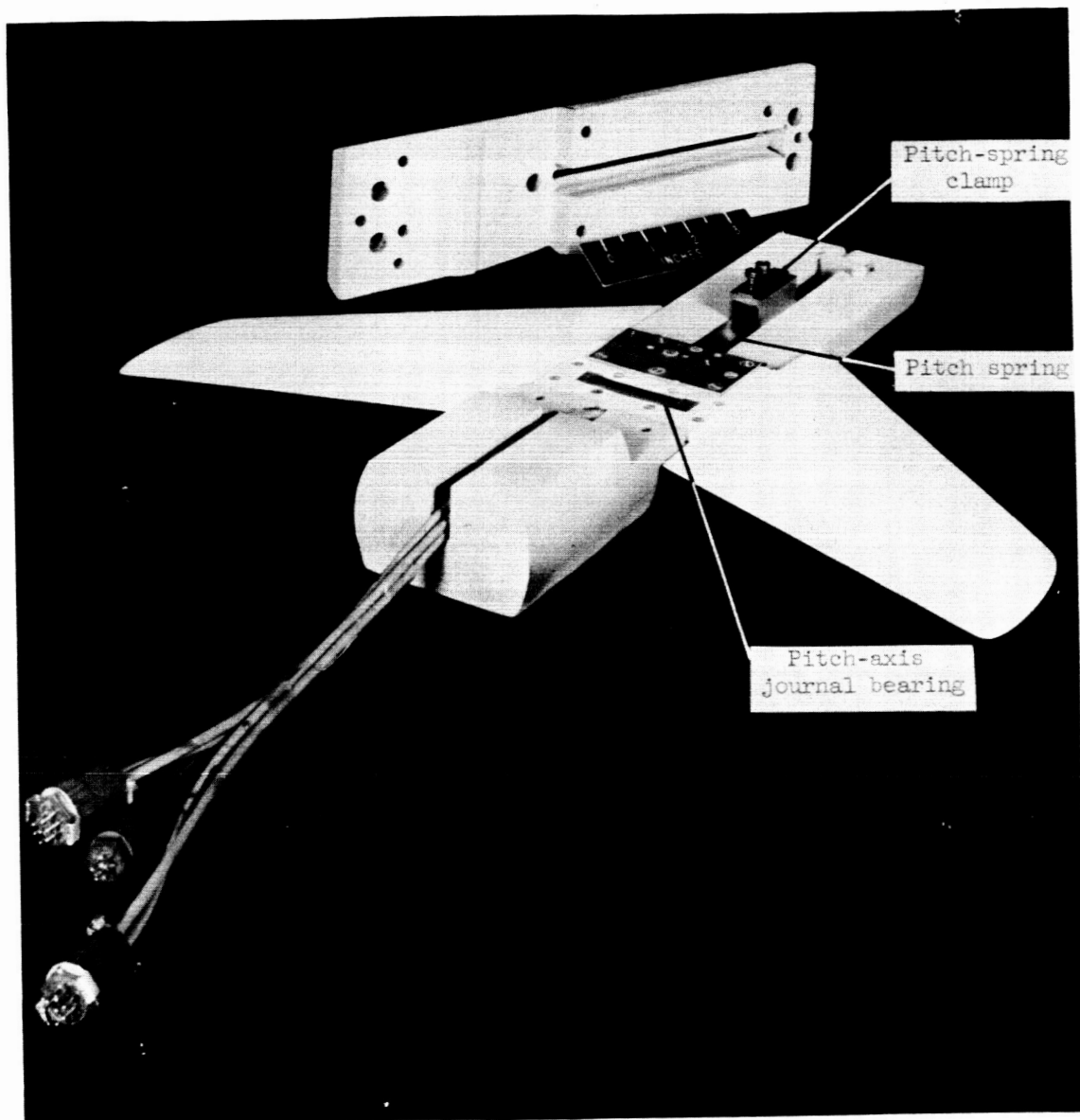


Figure 3.- Cross-sectional view through center line of model showing pitch roller and spring arrangement.

DECLASSIFIED



L-86671.1

Figure 4.- Model in partially assembled test fixture.

0371229 1030

NACA RM L56G06

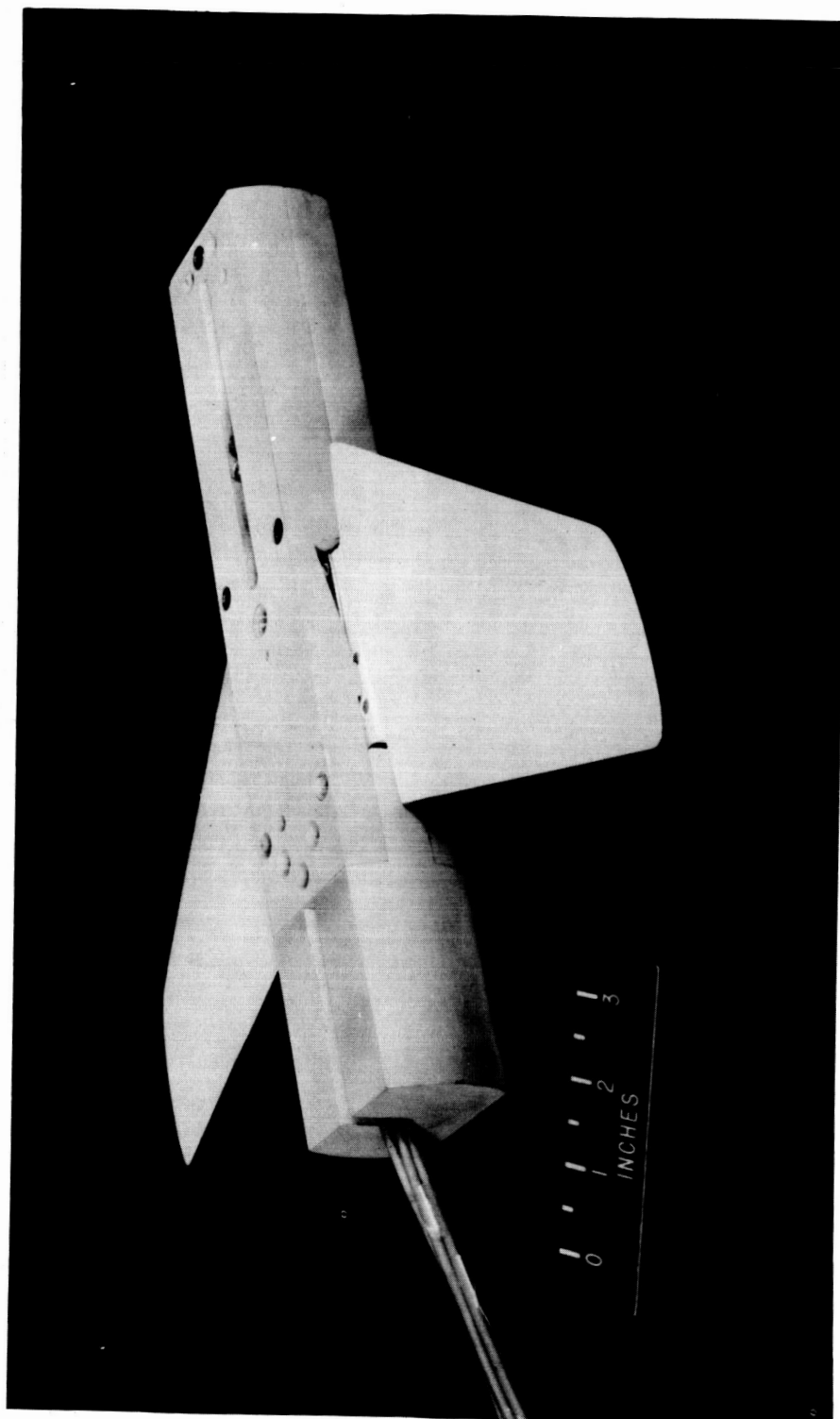


Figure 5.- Model in test fixture.

L-86670

DECLASSIFIED

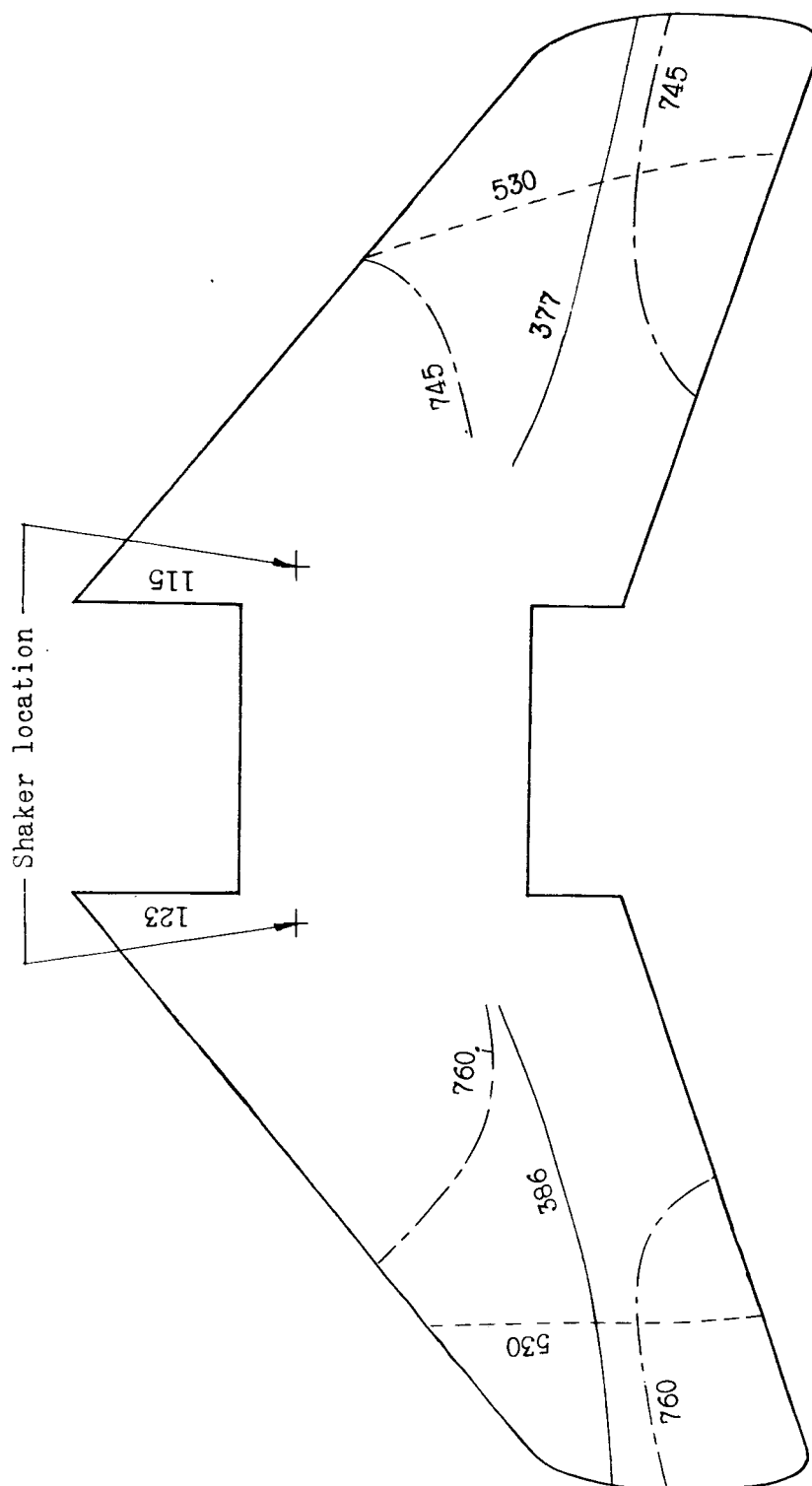


Figure 6.- Node lines and frequencies of horizontal-tail panels.  
Frequencies are in cycles per second.

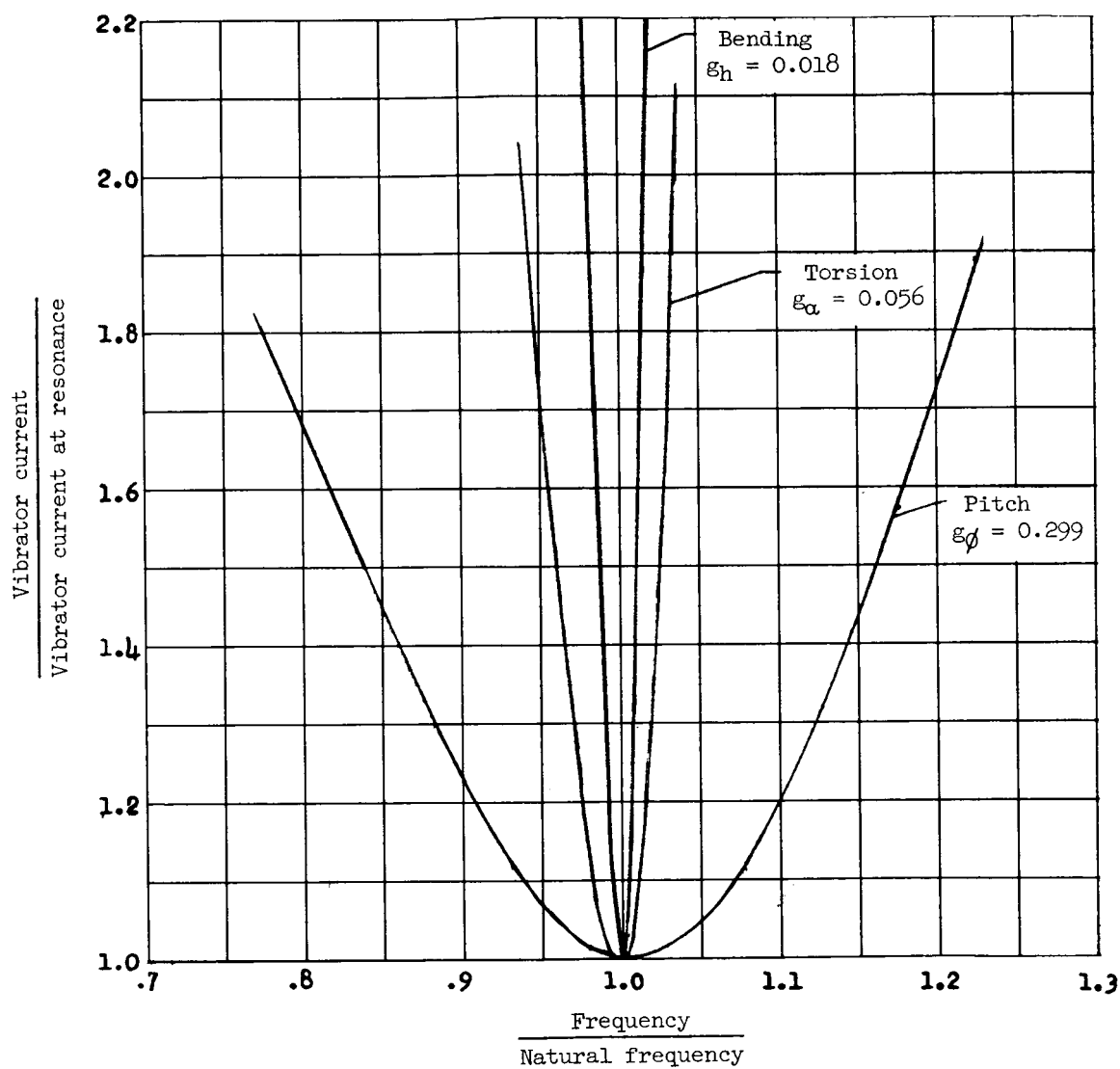


Figure 7.- Nondimensional frequency-response curves for model in bending, torsion, and pitch modes of vibration.

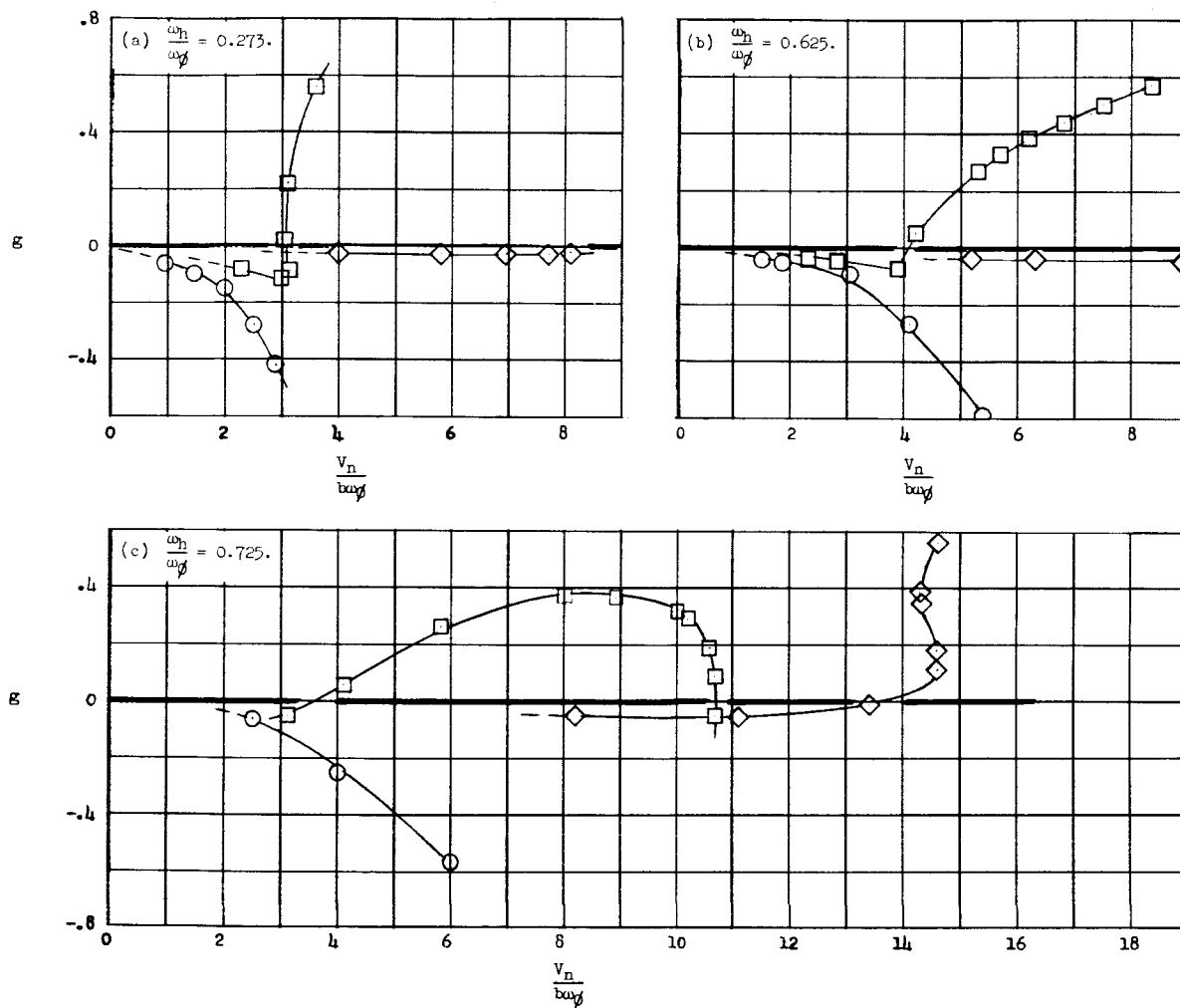
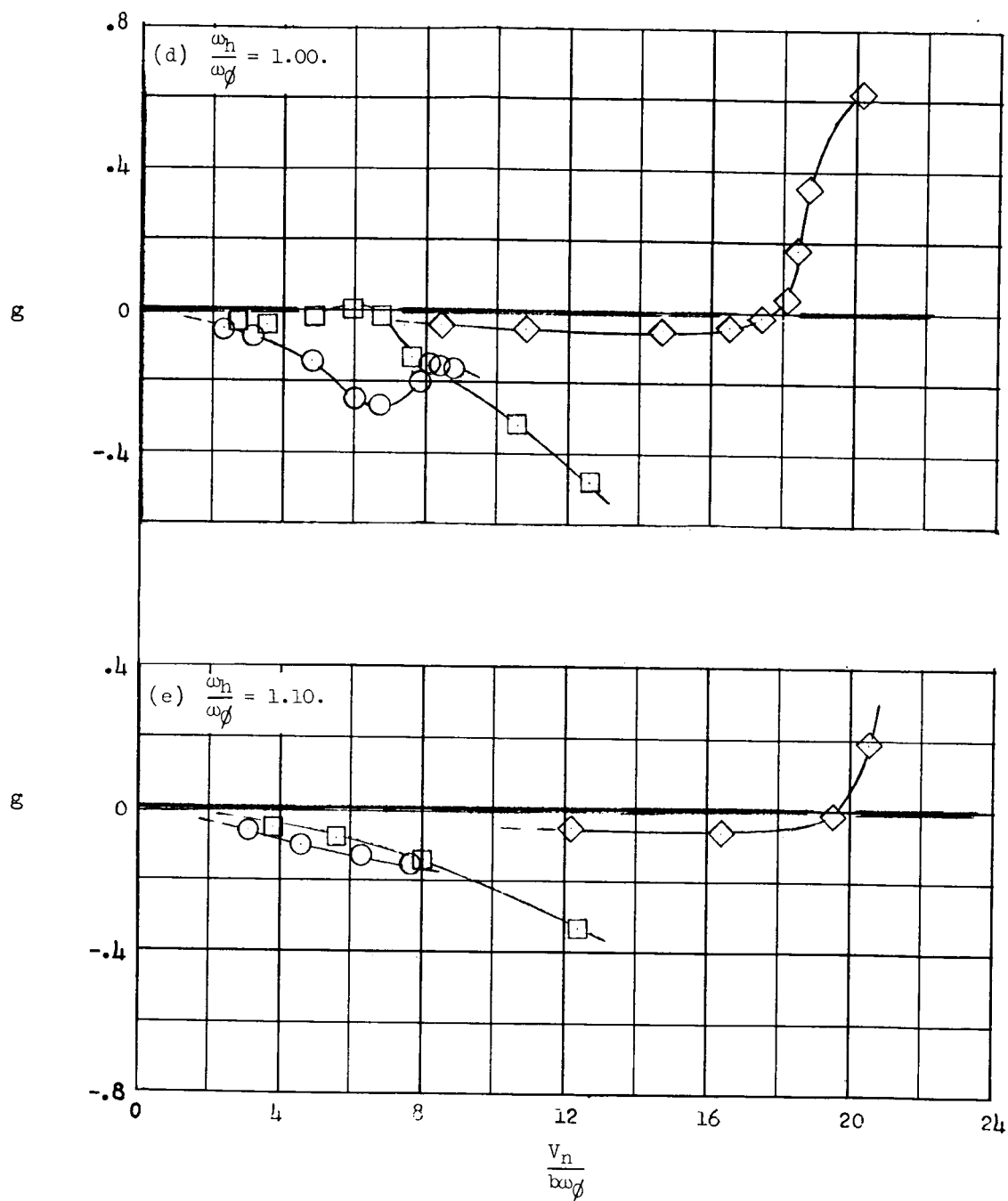


Figure 8.- Typical flutter solutions.  $\frac{\omega_n}{\omega_\alpha} = 0.305$ ;  $\rho = 0.0020$  slug/cu ft.



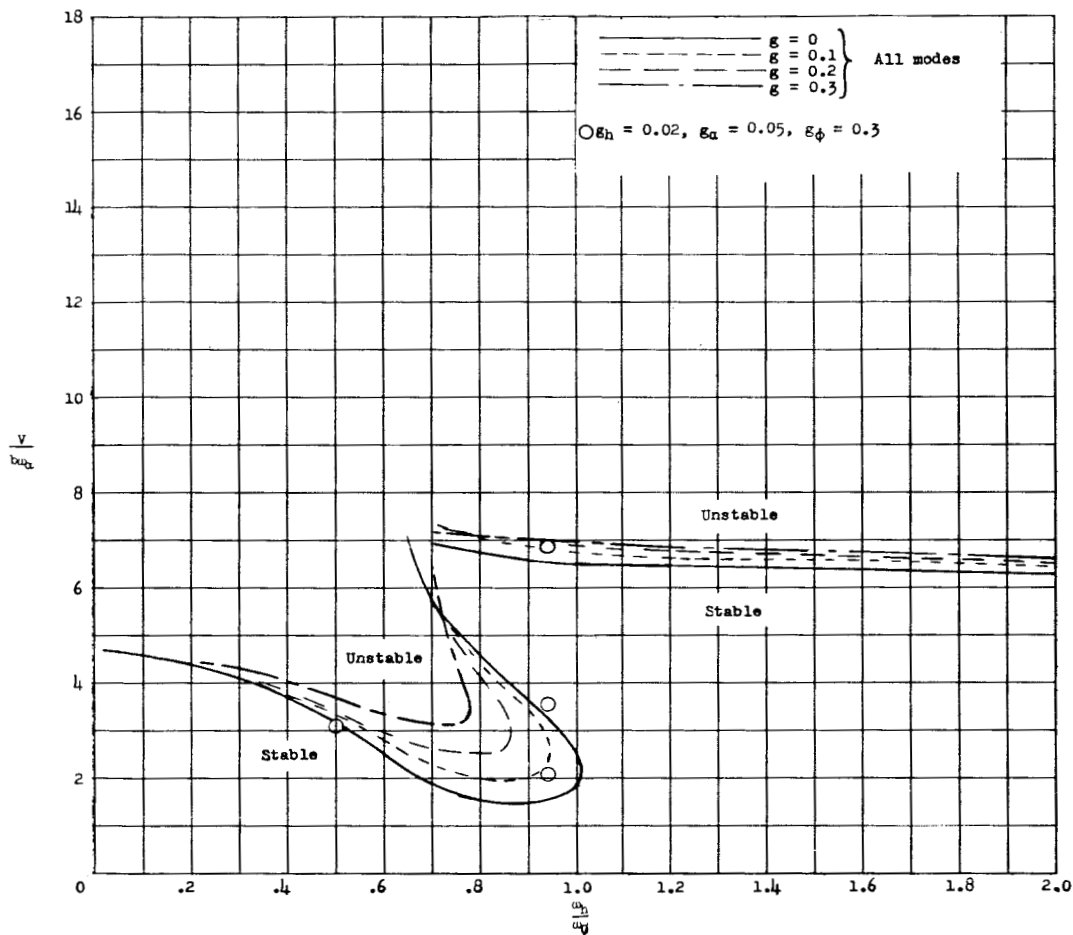


Figure 9.- Calculated flutter boundaries showing effect of frequency ratio  $\omega_h/\omega_\phi$  on reduced flutter speed  $V/b\omega_\alpha$ .  $\frac{\omega_h}{\omega_\alpha} = 0.305$ ;  $\rho = 0.0020$  slug/cu ft.



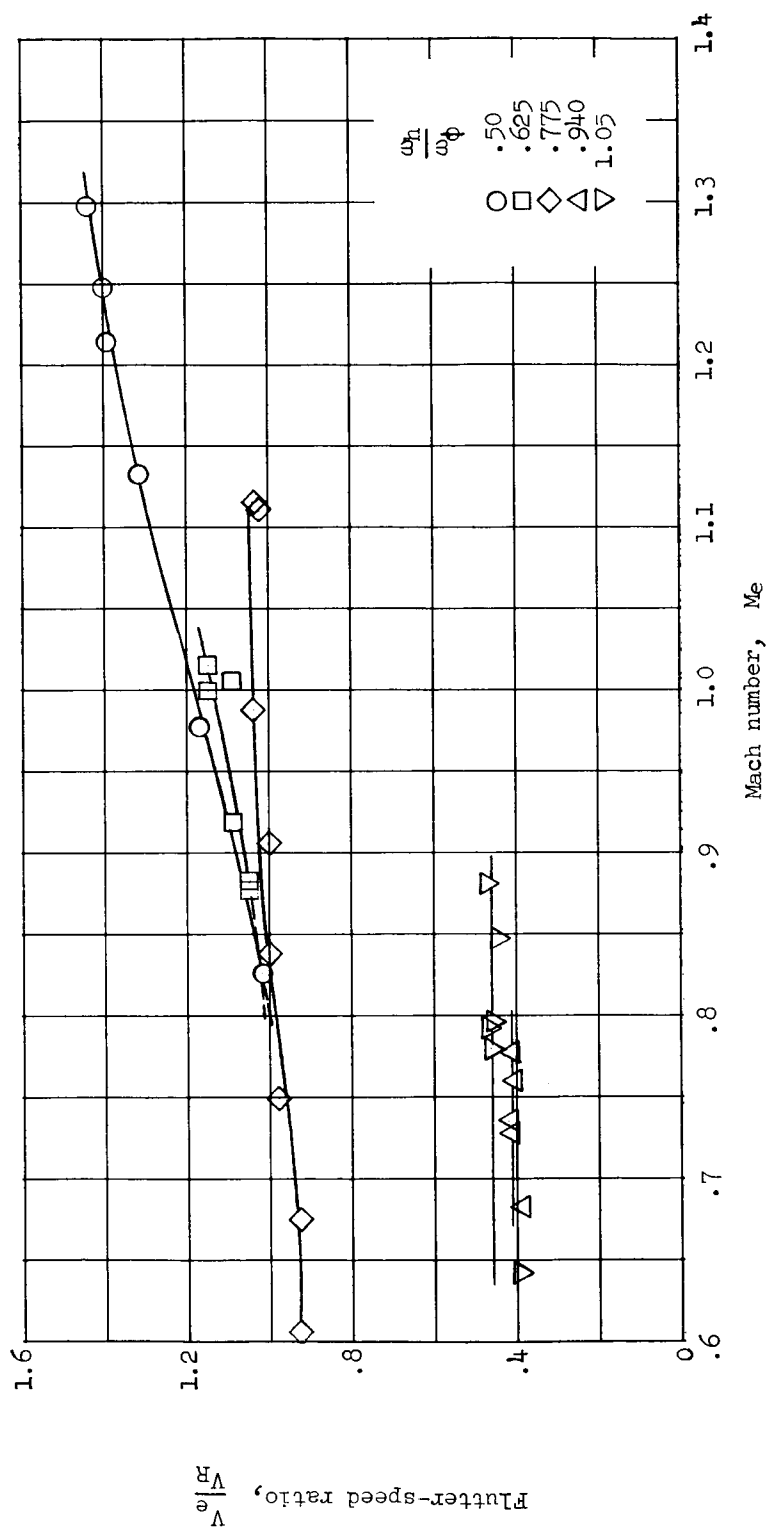


Figure 10.- Effect of Mach number on flutter-speed ratio.

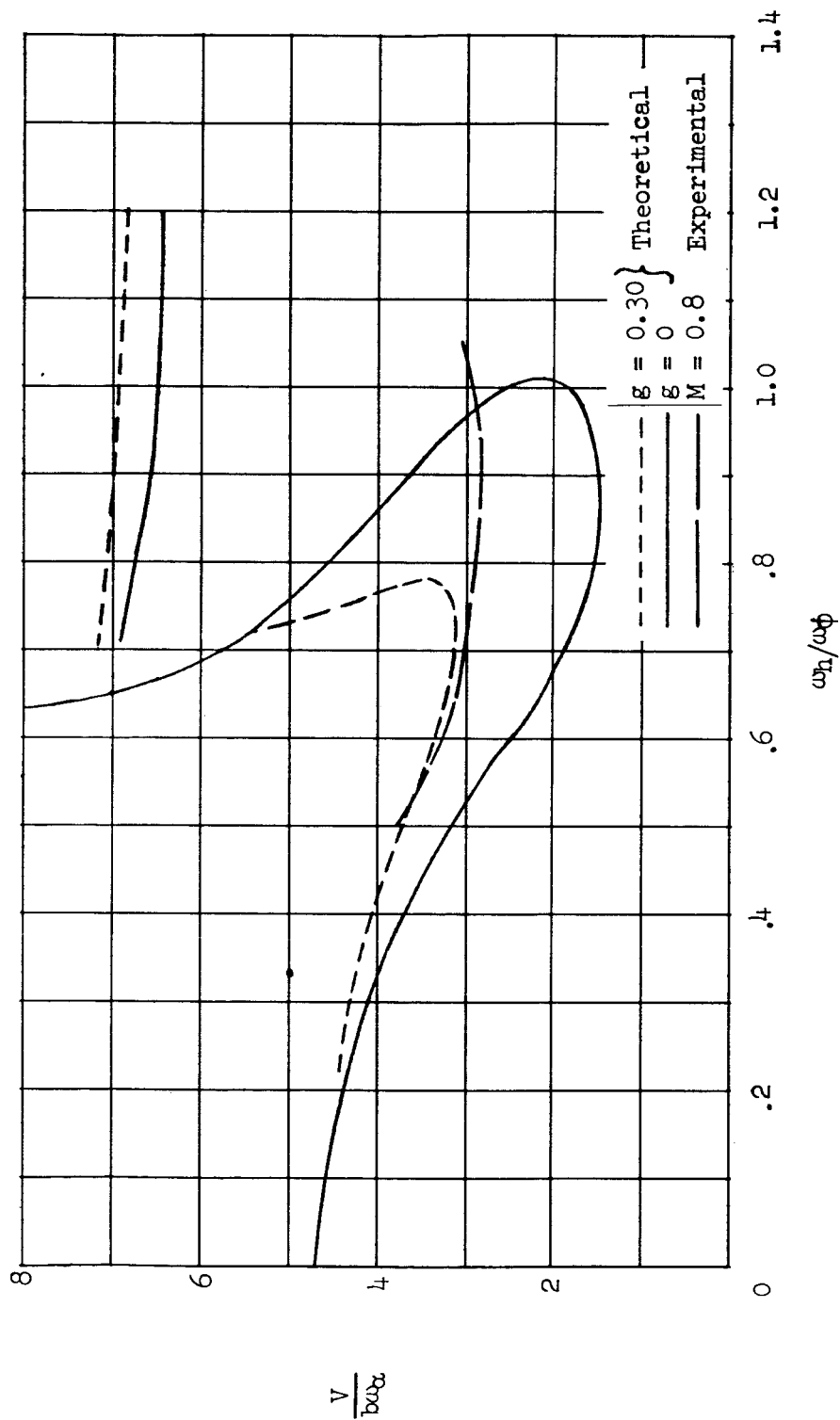


Figure 11.- Comparison of experimental and calculated flutter boundaries.